J. Meas. Sci. Instrum., 2024, 15(4): 532-546. http://jmsi.publish.founderss.cn
DOI: 10.62756/jmsi.1674-8042.2024053 jmsi@nuc.edu.cn

DC microgrid stability control with constant power load: a review

LI Xin[1*], ZOU Junnan[2], LIU Jinhui[2]

1.School of New Energy and Power Engineering, Lanzhou Jiaotong University, Lanzhou 730070, China;
2. School of Automation and Electrical Engineering, Lanzhou Jiaotong University, Lanzhou 730070, China

***Corresponding author:** LI Xin (lxfp167@163.com)

Received: September 3, 2023 **Revised:** October 17, 2023 **Accepted:** December 15, 2023

Abstract: The DC microgrid has the advantages of high energy conversion efficiency, high energy transmission density, no reactive power flow, and grid-connected synchronization. It is an essential component of the future intelligent power distribution system. Constant power load (CPL) will degrade the stability of the DC microgrid and cause system voltage oscillation due to its negative resistance characteristics. As a result, the stability of DC microgrids with CPL has become a problem. At present, the research on the stability of DC microgrid is mainly focused on unipolar DC microgrid, while the research on bipolar DC microgrid lacks systematic discussion. The stability of DC microgrid using CPL was studied first, and then the current stability criteria of DC microgrid were summarized, and its research trend was analyzed. On this basis, aiming at the stability problem caused by CPL, the existing control methods were summarized from the perspective of source converter output impedance and load converter input impedance, and the current control methods were outlined as active and passive control methods. Lastly, the research path of bipolar DC microgrid stability with CPL was prospected.

Key words: constant power load (CPL); DC microgrid; voltage balancer; stability criterion; cascaded system; virtual resistance

0 Introduction

Based on the method of energy conversion, microgrids are classified into three types as a critical component of the future intelligent power distribution system[1]. AC microgrids based on traditional AC transmission and distribution are more popular. Since more DC distributed power sources and DC loads have become available, the advantages of DC microgrids in power density, flexibility, and controllability over AC microgrids are becoming more apparent.

As indicated in Fig.1, DC microgrids have two power distribution structures: unipolar and bipolar[2,3], where bipolar microgrids can provide two voltage levels to the load. In a DC microgrid, the DC load is frequently linked to the source converter via the load converter, resulting in a cascade system[4-6]. Under closed-loop management, the load converter may be viewed as a CPL, and the negative resistance characteristic of the CPL can damage system stability and cause system voltage to fluctuate[7-9]. In essence, the stability issue produced by CPL is an impedance mismatch between the front and rear converters.

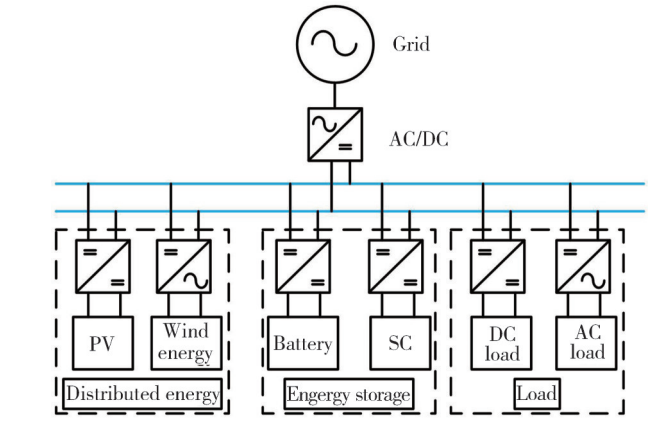

(a) DC microgrid structure in form of unipolar DC bus

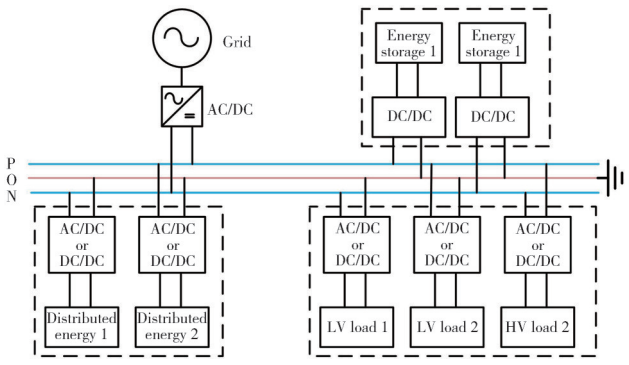

(b) DC microgrid structure in form of bipolar DC bus

Fig. 1 Distribution structure of DC microgrid

Many control methods have been presented to handle the DC microgrid stability problem caused by CPL, which may be split into two categories: active damping control and passive damping control.

Passive damping control will lead to significant energy loss compared to active damping control[10], whereas active damping control is a more suitable stability control strategy.

The stability of the DC microgrid has been the focus of attention. Meng analyzed the influence of control parameters on system stability by establishing a state-space averaging model of DC microgrid, and concluded that reasonable control parameters could effectively ensure the stability of the system[11]. Li focused on the stability of single-supply, single-load DC systems, and found that the dynamic changes in load power are an important cause of oscillations in DC voltage[2]. Yang focused on the study of sag-controlled DC microgrid stability problems, and obtained stable operating conditions applicable to microgrids of arbitrary structure by small perturbation approximation[3]. Rahimi implemented active damping based on inductor series virtual resistance in the control loop of the source converter by means of inductive current feedback, which reduced the output impedance resonance spikes of the source converter and thus achieved impedance matching of the front and rear stage converters[12].

In contrast, Zhang designed an active damping control method for the load converter, which adjusted the input impedance of the load converter by connecting virtual resistors in series and parallel. However, adjusting the output impedance of the load converter is complicated to implement in the control and may reduce the system reliability[13]. The DC microgrid with LC filter between front and rear converters was studied, respectively, and the corresponding stability control strategy was proposed. However, the existence of LC filter increased the hardware cost and system complexity[14,15]. These studies on the stability of DC microgrids are all based on unipolar DC microgrids, and there is a lack of systematic discussion on the stability of bipolar DC microgrids.

It is clear that the current research on bipolar DC systems lacks a discussion of stability problems caused by CPL. The stability problems faced by unipolar and bipolar DC microgrids were first analyzed, the idea of damping control implementation was refined, and Middlebrook stability criterion and other criteria for stability analysis were summarized.

1 Stability problem

The main factors affecting the stability of the DC microgrid are as follows.

1) The interaction between the converters.

2) When the converter is connected to CPL, the input side of converter has negative impedance characteristics in the control loop bandwidth.

3) The delay of the execution device and sensor, calculation, PWM signal, and phase-locked loop of the DC microgrid.

4) The voltage source converters have negative impedance characteristics in specific frequency ranges[16].

5) The control performance of the controller based on the small-signal model decreases under significant disturbance signals.

When the converter is designed separately, it can meet certain stability and dynamic performance requirements, but when multiple converters form a cascade system, the equivalent impedance parameters between the converters may be coupled and mismatched, resulting in instability of the whole system. Fig. 2 shows a block diagram of the cascade system, and the front and rear converters are called the source converter and the load converter, respectively.

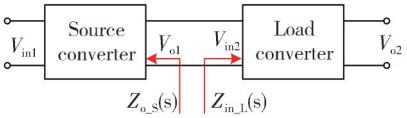

Fig. 2 Cascading system

As shown in the dotted line in Fig.3, Z_{o_S} is the output impedance of the source converter in the continuous current mode without considering the load resistance and the output impedance characteristics of Z_{o_S}, and LC is similar. f_{c_S} is the cut-off frequency of the voltage loop of the source converter. When $f < f_{c\_S}$, Z_{o_S} behaves as an inductance characteristic. When $f > f_{c\_S}$, the characteristic of Z_{o_S} is the same as that of the output filter capacitor of the source converter. When $f = f_{c\_S}$, $|Z_{o\_S}|$ has a peak $Z_{o\_S\_peak}$ and the $Z_{o\_S\_peak}$ is inversely proportional to the output filter capacitance of the source converter[17].

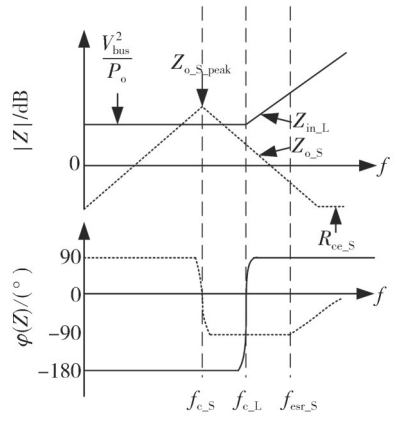

Fig. 3 Bode diagram of impedance intersection of cascaded system

As shown by the solid part of Fig. 3, Z_{in_L} is the input impedance of the load converter, where f_{c_L} is the cut-off frequency of the voltage loop of the load converter. When $f<f_{c\_L}$, Z_{in_L} behaves as a CPL. Its negative impedance expression is $-V_{bus}^2/P_o$, where V_{bus} is the intermediate bus voltage of the cascaded system, and P_o is the output power of the load converter. At this time, $|Z_{in\_L}|$ is inversely proportional to the magnitude of P_o. When $f>f_{c\_L}$, Z_{in_L} behaves as an inductance.

According to Fig. 3, if $|Z_{o\_S}|$ and $|Z_{in\_L}|$ intersect and $f_{c\_S}<f_{c\_L}$, the cascaded system is unstable. Moreover, the oscillation frequency of the cascaded system is about f_{c_S}, which has nothing to do with the power.

2 Stability criterion

2.1 Conventional stability criterion

To study the stability of DC microgrid, it is usually equated as a cascade system with the interaction of source converter and load converter. Among them, the middlebrook stability criterion is the first criterion proposed for analyzing stability[18].

However, because of its rigorous requirements, the concept of forbidden area is introduced and the GMPM (gain margin and phase margin) stability criterion is proposed[19]. Many criteria have been proposed based on the concept of the forbidden area[20-26]. And they all follow two principles.

1) The equivalent loop gain of the cascaded system satisfies the Nyquist criterion.

2) The criterion is practical.

It is assumed that the source and load converter of the cascaded system are stable when working alone and have good dynamic performance. As can be seen from Fig. 2, the transfer function $F(s)$ from the input to the output of the cascade system is

$$F(s)=\frac{V_{o2}}{V_{in1}}=G_1G_2\frac{Z_{in\_L}}{Z_{in\_L}+Z_{o\_S}}=\frac{G_1G_2}{1+T_m}, \quad (1)$$

where V_{o2} and V_{in1} are the output voltage and input voltage; G_1 and G_2 are the transfer functions of the source converter and the load converter; T_m is the equivalent impedance ratio of the converters.

Since G_1 and G_2 are assumed to be stable, T_m determines the stability of the cascaded system. According to the Nyquist criterion[27], the system is unstable if the impedance ratio amplitude-phase curve intersects with the unit circle and the surrounding point $(-1, j_0)$. In practice, if the loop gain intersects with the unit circle but does not surround the point $(-1, j_0)$, the stability of the system depends on whether the gain margin and phase margin of the system are large enough. The advantage of the impedance stability criterion is that it simplifies the stability problem of the system to whether the input and output characteristics of the source converter and the load converter match[28].

2.1.1 Middlebrook stability criterion

The Middlebrook stability criterion was proposed in 1976, which required $Z_{o\_S}(s)<Z_{in\_L}(s)$, namely

$$|T_m|=\left|\frac{Z_{o\_S}}{Z_{in\_L}}\right|\leqslant\left|\frac{1}{M_G}\right|<1, \quad (2)$$

where M_G is the gain margin.

It can be seen that if the Nyquist curve of T_m is in the unit circle, it will not surround the point $(-1, j_0)$, and the cascade system is stable.

Generally, $M_G=2$ and the Nyquist curve of T_m is limited to a circle with a radius of $1/M_G$ to ensure the stability of the system in Fig. 2. The area outside the unit circle is the forbidden area of T_m as shown in Fig. 4.

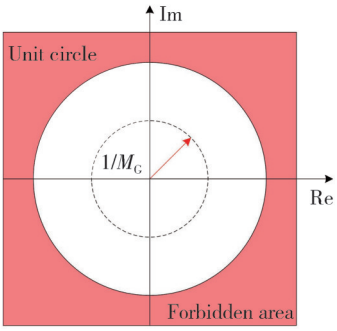

Fig. 4 Middlebrook stability criterion restricted area

The Middlebrook criterion only considers the amplitude margin of T_m without considering the phase margin, which gives it some limitations and conservativeness.

2.1.2 GMPM stability criterion

The stability criterion of GMPM based on restricted area means that a restricted area is set in the complex plane.

$$\begin{cases} T_m=\dfrac{Z_o}{Z_{in}}\geqslant\dfrac{1}{M_G}, \\ \left[\arg(Z_o)-\arg(Z_{in})\right]\leqslant 180^\circ-M_P, \end{cases} \quad (3)$$

where M_P is the phase margin.

The forbidden area of the GMPM stability criterion is shown in Fig. 5. As long as T_m does not enter this region, the system is considered stable and the cascaded system has the desired M_P and M_G. In practical engineering applications, $M_P=60^\circ$ and $M_G\geqslant 2$ are taken into account the changes of actual parameters.

The GMPM stability criterion overcomes the conservatism of Middlebrook stability criterion to some extent, reduces the limit area of system parameter

design, increases the degree of freedom of system parameter design, and only needs the amplitude and phase information of source converter and load converter.

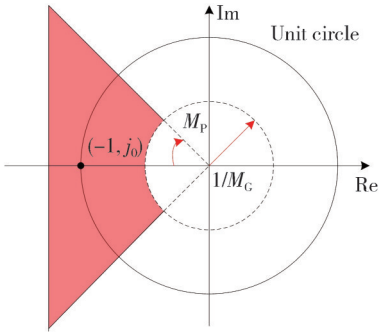

Fig. 5 GMPM stability criterion forbidden area

2.1.3 OA stability criterion

Based on the GMPM stability criterion, the OA (Opposing argument) stability criterion is proposed, as shown in Fig.6.

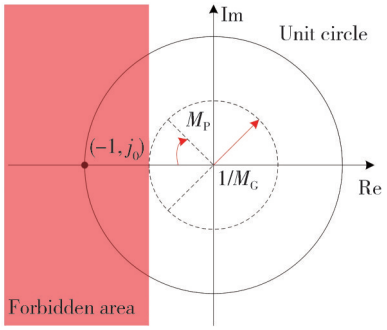

Fig. 6 OA stability criterion forbidden area

The forbidden area of the OA stability criterion is

$$\mathrm{Re}(T_m) \leqslant -\frac{1}{M_G}. \tag{4}$$

For the cascaded system shown in Fig.7, in which one source converter supplies power to n load converters, $Z_{in}=Z_{in1}\|\cdots\|Z_{inn}$, and the secondary loop gain is

$$T_m = \frac{Z_o}{Z_{in}} = \frac{Z_o}{Z_{in1}} + \frac{Z_o}{Z_{in2}} + \frac{Z_o}{Z_{in3}} + \cdots + \frac{Z_o}{Z_{inn}}. \tag{5}$$

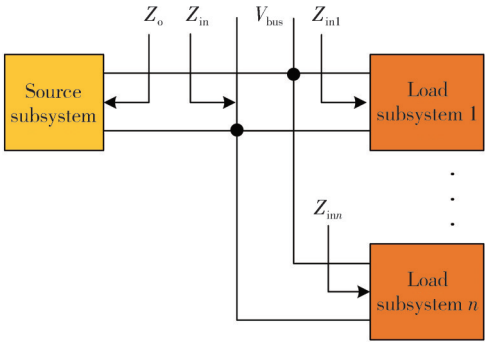

Fig. 7 DCDPS with one source subsystem supplying n load subsystems

Suppose the power of source subsystem is P_o, the power of n load subsystem are P_{in1}, P_{in2}, $\cdots$, P_{inn}, and they satisfy

$$P_o \geqslant P_{in1} + P_{in2} + P_{in3} + \cdots + P_{inn}. \tag{6}$$

Then the forbidden area of the sub-loop gain Z_o/Z_i $(k=1,2,\cdots,n)$ of each load subsystem is

$$\mathrm{Re}(T_m) = \mathrm{Re}\left(\frac{Z_o}{Z_{ink}}\right) \leqslant -\frac{1}{M_G}\frac{P_{ink}}{P_o}. \tag{7}$$

The forbidden area criterion is suitable for the case of multi-load converters. As long as T_m does not fall within the forbidden area, the system can remain stable when multiple converters are connected in parallel and cascaded with the source converter[29].

2.1.4 MP stability criterion

The amplitude margin and phase margin can ensure the relative stability of the system, but when the Nyquist curve of T_m is close to the point $(-1, 0)$, the relative stability decreases. Therefore, the amplitude margin and phase margin do not guarantee the relative stability of the system. In this regard, the MP (Maximum peak) stability criterion defines the distance from the Nyquist curve of T_m to the point $(-1, 0)$, which can ensure that the system has a certain stability margin. The forbidden area of the circle with the point $(-1, 0)$ as its center and R_0 as its radius can ensure the system's stability margin. The forbidden area is shown in Fig.8.

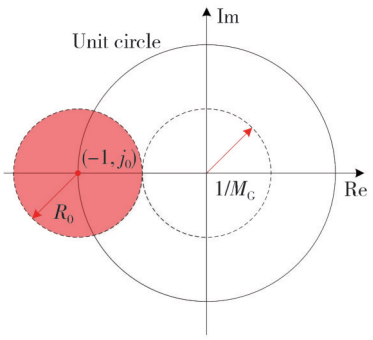

Fig. 8 MP stability criterion forbidden area

The forbidden area can be expressed as

$$\begin{cases} M_P \geqslant 2\arcsin\dfrac{R_0}{2} \geqslant R_0, \\ M_G \geqslant \dfrac{1}{1-R_0}\left(20\lg\dfrac{1}{1-R_0}\right). \end{cases} \tag{8}$$

The MP stability criterion can monitor the DC microgrid's stability margin online by adding small-signal voltage disturbances to the DC bus. The MP stability criterion is mainly used to judge the stability of the DC microgrid when the system parameters change slightly[30].

2.1.5 ESAC stability criterion

As illustrated in Fig. 9, the energy source analysis consortium (ESAC) stability criterion banned region consists of two straight lines beginning at infinity parallel to

the real axis and ending at the unit circle, and two straight lines beginning at the unit circle and ending at $s=-1/M_G$. The ESAC forbidden area is generally set to meet the system's stable operation with $M_G=2$ and $M_P=60°$. The ESAC stability criterion applies to the design of the load impedance for a given source impedance. A three-dimensional admittance space can describe the stability with frequency, phase, and amplitude as the three axes[31,32]. The ESAC stability criterion can set the appropriate phase margin and amplitude margin according to the stable operation requirements of the DC microgrid. The area of the exclusion zone given by the ESAC stability criterion varies with the phase margin and amplitude margin.

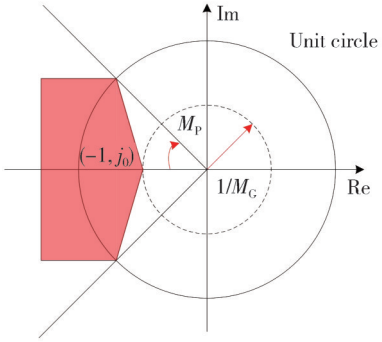

Fig. 9 ESAC stability criterion forbidden area

In the case of the same phase margin and amplitude margin, the ESAC stability criterion has a smaller forbidden area than other criteria and relatively tiny conservativeness.

2.1.6 RES stability criterion

As shown in Fig.10, root exponential stability (RES) is similar to ESAC, and they differ less in terms of design. Compared to ESAC, RES stability criterion is superior in calculating the load conduction constraint based on the source impedance, while the RES stability criterion forbidden region is expressed as a continuous function[33].

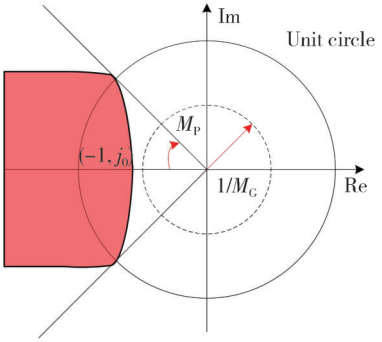

Fig. 10 RES stability criterion forbidden area

The RES stability criterion can be defined by introducing

$$f(s)=\sqrt[n]{\left[\alpha\,\mathrm{Im}(s)\right]^n+\left[\beta e^{\gamma \mathrm{Re}(s)}\right]^n}, \tag{9}$$

where $n\geqslant 2$ and it is an even integer; $\mathrm{Re}(s)$ and $\mathrm{Im}(s)$ are the real and imaginary parts of the complex variable, respectively; α, β, and γ are positive real constants.

The RES stability criterion exclusion zone is defined by the set of points satisfying the s-plane.

$$f(s)=1. \tag{10}$$

Then there are

$$\begin{cases}\alpha=\dfrac{1}{\sqrt[n]{2}\,\sin M_P{}^*},\\ \beta=\dfrac{1}{\sqrt[n]{2}}e^{\gamma\cos M_P{}^*},\\ \gamma=\dfrac{M_G{}^*\ln\sqrt[n]{2}}{M_G{}^*\cos M_P{}^*-1},\end{cases} \tag{11}$$

where $M_G{}^*\cos M_P{}^*>1$.

The additional performance of the RES stability criterion can be expressed as

$$f(s)=\sqrt[n]{(\alpha x)^n+(\beta y)^n}, \tag{12}$$

where $x=e^{\gamma \mathrm{Re}(s)}$, $y=\mathrm{Im}(s)$.

It can be known that RES is a hyperellipse. In addition, when $x>0$, the forbidden region of the RES stability criterion in the s-plane is not closed. When $\mathrm{Re}(s)$ tends to negative infinity and x tends to zero, the forbidden area of the RES criterion becomes a horizontal line, that is

$$\mathrm{Im}(s)\to\pm\frac{1}{\beta}. \tag{13}$$

2.1.7 T-SI stability criterion

The T-SI stability criterion is to study the small-signal stability problem of the system shown in Fig.7. It is assumed that all regulated subsystems are PWM-controlled DC/DC converters, and the load impedance of the kth load subsystem is denoted as R_k.

The mapped pure impedance Z_k of the kth load subsystem is defined as

$$Z_k=\begin{cases}R_k, & \text{for unregulated load subsystems},\\ R_k{D'_k}^2, & \text{for boost-type load subsystems},\\ R_k/{D_k}^2, & \text{for buck-type load subsystems},\end{cases} \tag{14}$$

where D_k is the steady-state step-down ratio of the kth buck-type load subsystem; $1/D_k$ is the steady-state step-up ratio of the boost-type load subsystem. The equivalent mapped pure impedance Z of n parallel load subsystems is expressed as

$$\frac{1}{Z}=\frac{1}{Z_1}+\frac{1}{Z_2}+\cdots+\frac{1}{Z_k}+\cdots\frac{1}{Z_n}. \tag{15}$$

The T-SI stability criterion breaks through the conservatism of the criterion because it does not assume that G_1 and G_2 in Eq. (1) must be stable transfer

functions. If the sub-loop gain of Eq. (1) is used, an incorrect stability judgment will be produced in an unstable independent source subsystem. Therefore, the impedance criterion does not apply to the sub-loop gain, but the extended sub-loop gain is used.

$$T_{\mathrm{m}}=Z_{\mathrm{o}}(s)\left[\frac{1}{Z_{\mathrm{in}}(s)}-\frac{1}{Z(s)}\right], \tag{16}$$

where $Z_{\mathrm{o}}(s)$ is the output impedance of the source subsystem; $Z_{\mathrm{in}}(s)$ is the equivalent input impedance of all n load subsystems in parallel.

The T-SI stability criterion includes three steps.

1) The stability of the system is analyzed by the load subsystem and the corresponding mapped impedance.

2) The output impedance of the source subsystem connected to the mapped pure impedance is measured first, and then the input impedance of each load subsystem is measured.

3) For the DC microgrid shown in Fig.7, the Nyquist curve of T_{m} is used to judge the system stability.

2.2 General stability criterion

In practice, in addition to the cascade form, there are more complex forms of DC microgrid connections, as shown in Fig.11.

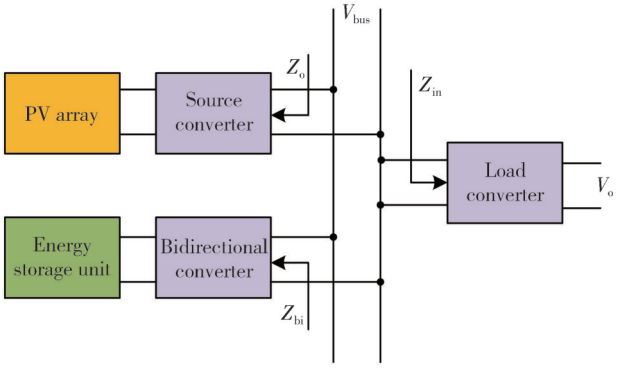

Fig. 11 DCDPS with power generation and energy storage unit

When the energy provided by PV array is insufficient to meet the energy requirements of the load, the bidirectional converter replenishes the energy from the battery to the load converter, which acts as a source converter. And when the energy provided by the PV array exceeds the energy requirements of the load, the excess energy is stored in the battery via the bidirectional converter, which acts as a load converter.

Therefore, if the impedance criterion above is used to determine the stability of the system, it is necessary to consider the two system operation modes. The PV array is insufficient to provide the energy required by the load, and the PV array is larger than the energy required by the load, which makes the analysis of the system stability problem more difficult.

The converters in the DC microgrid are classified as BVCCs (Bus voltage-controlled converters) and BCCCs (Bus current-controlled converters)[34]. BVCC refers to the converter that directly or indirectly controls its port voltage V_{bus} on the DC bus side of the system, as shown in Fig.12(a). BCCC refers to the converter that directly or indirectly controls its port current I_{bus} on the DC bus side of the system, as shown in Fig.12 (b).

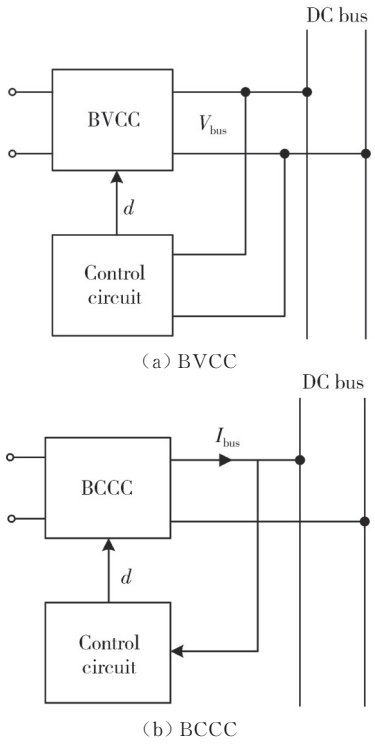

Fig. 12 BVCC and BCCC

The converters that control the port voltage or port current on the bus side are divided into BVCC and BCCC[35], so the unified form of the DC microgrid can be obtained as shown in Fig. 13. $m\,(m\geqslant 1)$ BVCCs are connected in parallel on the DC bus to control the port voltages on their respective bus sides. $n\,(n\geqslant 1)$ BCCCs are connected in parallel on the DC bus to control the port currents on their respective bus sides. $I_{\mathrm{busv}j}$ $(j=1,2,\cdots,m)$ and $I_{\mathrm{busc}k}$ $(k=1,2,\cdots,n)$ are the port currents on the bus side of the jth BVCC and the kth BCCC, respectively.

Using the DC microgrid two-port small signal model to determine $Z_{\mathrm{busv}j}$ and $Z_{\mathrm{busc}k}$, the equivalent gain of the DC microgrid cascade loop can be obtained by

$$T_{\mathrm{m}}=\frac{Z_{\mathrm{busv}}}{Z_{\mathrm{busc}}}=\frac{\left(\sum_{j=1}^{m}\frac{1}{Z_{\mathrm{busv}j}}\right)^{-1}}{\left(\sum_{k=1}^{n}\frac{1}{Z_{\mathrm{busc}k}}\right)^{-1}}. \tag{17}$$

The steps to determine the stability of DC microgrids

according to the generic impedance criterion are as follows[36].

1) The DC microgrid is transformed into a unified form to determine the number of BVCC and BCCC in the system.

2) The port impedance values m and n of BVCC and BCCC are substituted into Eq. (17).

3) The stability of the system is determined according to whether the T_m meets the Nyquist criterion.

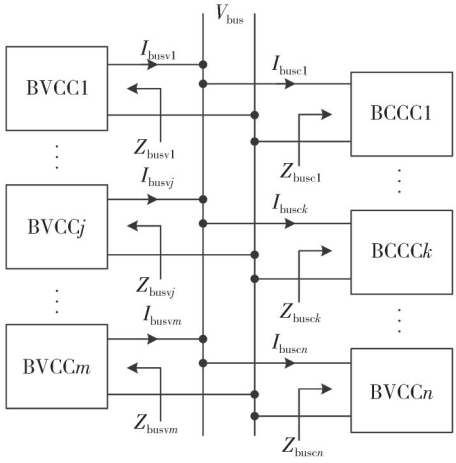

Fig. 13 Unified Form

2.3 Bipolar stability criterion

The above stability criterion can only describe the impedance-matching relationship of the unipolar DC microgrid. In the bipolar DC system, due to unbalanced conditions, the change of the output impedance of the source converter to the load converter is different from that of the unipolar system. Specifically, when the negative load changes, the output impedance of the source converter to the positive electrode changes, and vice versa. In a unipolar system, the load change does not change the output impedance of the source converter. For a bipolar DC system, referring to Eq. (2), the Middlebrook stability criterion can be described as

$$\begin{cases} T_{p\_m} = \dfrac{|Z_{p\_o}|}{|Z_{p\_in}|} \ll 1, \\ T_{n\_m} = \dfrac{|Z_{n\_o}|}{|Z_{n\_in}|} \ll 1, \end{cases} \tag{18}$$

where Z_{p_in} and Z_{n_in} are the closed-loop input impedance of the positive load converter and the negative load converter; Z_{p_o} and Z_{n_o} are the closed-loop output impedance of the source converter to the positive load and the negative load.

It can be seen that the bipolar DC microgrid needs both the positive side and the negative side to satisfy the Middlebrook stability criterion. Moreover, due to the existence of unbalanced working conditions, in the system stability analysis, bipolar DC microgrids need to consider more situations than unipolar DC microgrids. Therefore, the bipolar DC microgrid is more complicated than the unipolar DC microgrid when using the Middlebrook stability criterion for stability analysis and stability control method design[37].

According to the existing stability criterion, it is known that the equivalent loop gain of the cascaded system satisfies the Nyquist criterion is necessary to ensure the stable operation of the system. Based on this idea, many different control methods have been proposed for the stability of DC microgrids, which can be broadly classified into two categories: passive damping control methods and active damping control methods. The typical characteristics of the methods mentioned below are shown in Table 1.

Table1 Typical characteristics of various methods

Control strategy	Methods	Typical characteristics
Passive damping control	R_d-C_d parallel	Excellent dynamic performance with extra losses
	R_d-L_d series	
	R_d-L_d parallel	
	Busbar is connected in parallel with C_{bus}	Deterioration of dynamic performance
Active damping control	Active capacitive converter control	Has strong adaptability
	Virtual resistor active damping control	Guaranteed dynamic performance while solving stability problems

3 Passive damping control method

The passive damping control method improves the damping characteristics of the system by incorporating a damping loop to reduce the output impedance of the source converter or increase the input impedance of the load converter, thus reducing the cross-cutting range of the input and output impedances. When the converter is well controlled, its input impedance frequently exhibits negative impedance characteristics in the low-frequency range, which frequently interacts with the output impedance of the input filter, causing system instability. Four passive damping control methods are summarized for DC microgrid cascade system stability problems, as shown in Fig.14.

1) An R_d-C_d damping branch is connected in parallel to the filter capacitor of the LC filter[38].

2) An R_d-L_d damping branch is connected in series with the filter inductor of the LC filter[39].

3) An R_d-L_d damping branch is connected in parallel to the filter inductor of the LC filter[40,41].

The three methods adjust the resonant peak of the

output impedance by damping filter to avoid amplitude crossover, which makes the amplitude-phase curve of the equivalent loop gain of the cascaded system always within the unit circle and ensures the system stability, but these three passive control methods also cause additional losses.

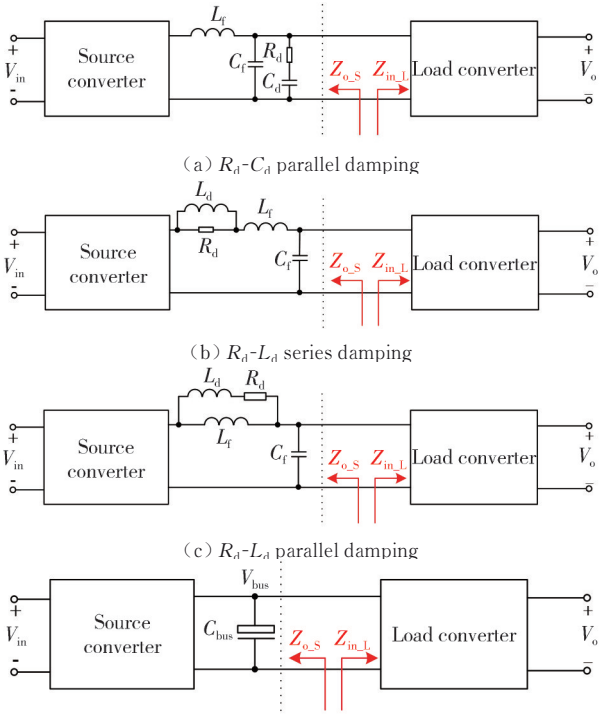

(a) R_d-C_d parallel damping

(b) R_d-L_d series damping

(c) R_d-L_d parallel damping

(d) Busbar is connected in parallel with C_{bus}

Fig. 14 Passive control methods

In Fig. 14(d), an additional bus capacitor C_{bus} is connected in parallel between the input filter and the converter. The purpose is to reduce the amplitude of the output impedance of the input filter in the full frequency range, thereby avoiding amplitude crossover of the cascaded system and ensuring system stability[42].

4 Active damping control method

Although the passive damping control methods can solve the instability of the cascade system, the existence of damping devices will increase system losses, reduce system efficiency, and increase the size and weight of the system, which will undoubtedly increase the cost of the system and is not conducive to the improvement of the system power density. Therefore, the active damping control methods are more widely used[43-47].

4.1 Active capacitive converter control

The ideal situation for a cascading system to work stably is when $|Z_{o\_S}|$ and $|Z_{in\_L}|$ do not intersect. $|Z_{o\_S\_peak}|$ is inversely proportional to the size of the output filter capacitor of the source converter. The output filter capacitor of the source converter, that is the intermediate bus capacitor C_{bus} of the system, can be increased to avoid the intersection of $|Z_{o\_S}|$ and $|Z_{in\_L}|$, as shown in Fig.15.

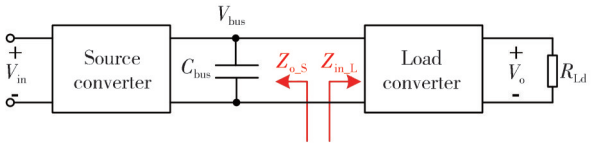

Fig. 15 Cascading system after adding C_{bus}

According to the analysis above, it is known that Z_{o_S} is similar to the characteristics of LC filter, so for the convenience of analysis, the equivalent inductance of the LC filter is defined as L_{e_S}, the equivalent capacitance is C_{e_S}, the parasitic resistance of L_{e_S} is R_{le_S}, and the parasitic resistance of C_{e_S} is R_{ce_S}. Then, according to Fig.3, the expressions of R_{ce_S}, C_{e_S}, L_{e_S}, and R_{le_S} can be derived as

$$R_{ce\_S}=\left|Z_{o\_S}(f_{esr\_S})\right|, \tag{19}$$

$$C_{e\_S}=\frac{1}{2\pi R_{ce\_S}f_{esr\_S}}, \tag{20}$$

$$L_{e\_S}=\frac{1}{(2\pi f_{c\_S})^2 C_{e\_S}}, \tag{21}$$

$$R_{le\_S}=\frac{L_{e\_S}}{C_{e\_S}\left|Z_{o\_S\_peak}\right|}-R_{ce\_S}, \tag{22}$$

where f_{esr_S} is the frequency of the zero point formed by R_{ce_S} and C_{e_S}.

When C_{bus} is considered, the equivalent circuit model of Z_{o_S} is shown in Fig.15. Fig.16 shows the equivalent model of output impedance of source converter considering C_{bus}.

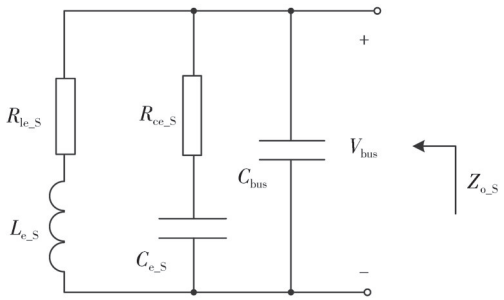

Fig. 16 Equivalent model of output impedance of source converter considering C_{bus}

According to Eqs. (19)—(22) and Fig. 16, the expression of $|Z_{o\_S\_peak}|$ can be deduced as

$$\left|Z_{o\_S\_peak}\right|=\frac{L_{e\_S}}{(C_{e\_S}+C_{bus})(R_{le\_S}+R_{ce\_S})}. \tag{23}$$

If Z_{o_S} is to be less than Z_{in_L} over the full frequency range, $|Z_{o\_S\_peak}|$ must satisfy

$$\left|Z_{o\_S\_peak}\right| \leqslant \frac{V_{bus}^2}{P_o}. \tag{24}$$

Combining Eqs. (23) and (24), C_{bus} must satisfy

$$C_{bus} \geqslant \frac{L_{e\_S}P_o}{V_{bus}^2\left(R_{le\_S}+R_{ce\_S}\right)} - C_{e\_S}. \tag{25}$$

According to Eq. (25), the more significant P_o value, the larger the bus capacitance required to ensure the stability of the cascaded system. Therefore, C_{bus} must be selected at full load. Since the capacitance value is generally relatively large, it will reduce the cut-off frequency of the voltage loop of the source converter and make its dynamic response speed slower. Moreover, the capacitor is generally chosen as an electrolytic capacitor, which has a short service life and is the main component that limits the service life of the converter.

Assuming that the capacitance value of C_{bus} can be adaptively changed with P_o, it is the minimum value to ensure the stability of the cascade system under any load conditions. In that case, the problem caused by the increase of the intermediate bus capacitance control method can be solved. In practice, C_{bus} can be realized by a converter, that is an active capacitive converter[48].

The circuit topology of the active capacitor converter control (AACC) is shown in Fig. 17. It consists of switch tubes Q_{a1}, Q_{a2}, inductor L_a, and capacitor C_a. The output port of the AACC is connected in parallel with the intermediate DC bus.

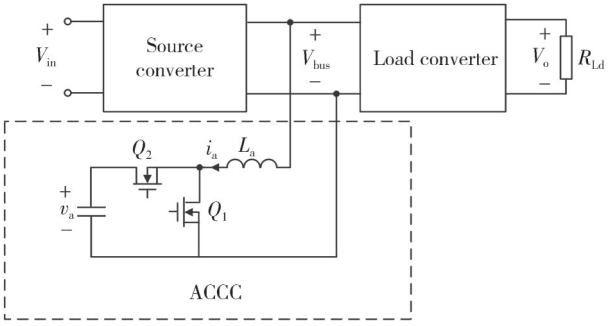

Fig. 17 Cascade system after introducing ACCC

The working principle of the active capacitor converter is that the current of L_a is controlled according to the bus voltage V_{bus} of the system, so that the port characteristic of the bus side of ACCC is represented as a C_{bus} whose capacitance value changes adaptively with P_o. In this way, the cascaded system can work stably in the entire load range and have a faster dynamic response speed.

The ACCC is suitable for the cascaded system of single-load converters and the cascaded system of multi-load converters. The bus capacitance can effectively reduce the closed-loop output impedance amplitude of the source converter, avoid its intersection with the input impedance of the load converter system, and ensure the stability of the cascade system[49].

Experiments are carried out on a 120 W unstable buck-buck cascade system to verify the effectiveness of the active capacitor converter[50].

As can be seen from Fig. 18, neither the intermediate bus voltage nor the output voltage oscillates after the active capacitor converter is added. It shows that the active capacitance converter can effectively solve the stability problem of the system at full load.

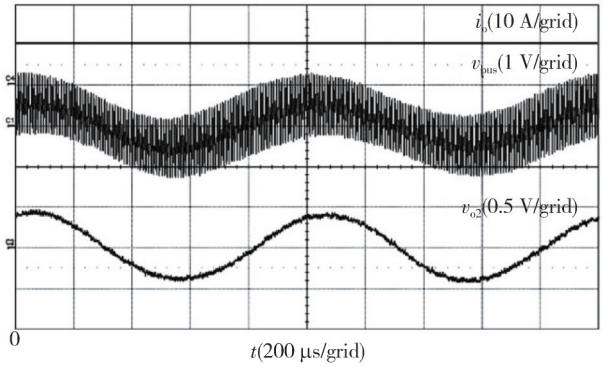

(a) Before adding the active capacitor converter

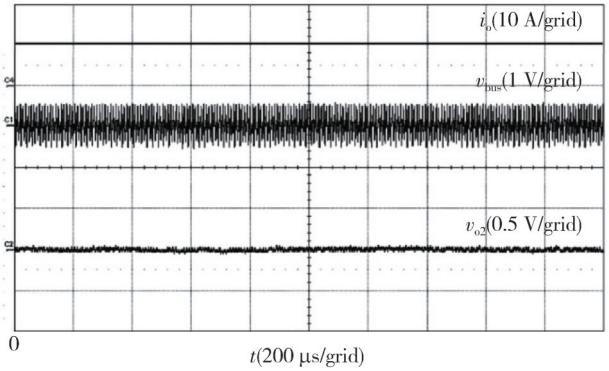

(b) After adding the active capacitor converter

Fig. 18 Control effect of ACCC under full load

Fig. 19 shows the control effect of ACCC under half load. It demonstrates that after the active capacitor converter is added, neither the intermediate bus voltage nor the output voltage oscillates, indicating that the active capacitor converter effectively solves the stability problem when the system is half-loaded.

This example demonstrates that the active capacitor converter solves the system's stability problem and has strong adaptable qualities. It has high practical utility and application potential in the cascade system.

When the peak value of the source converter output impedance is within the cutoff frequency of the load converter voltage loop gain or intercepted with the input impedance of the load converter, it will cause system instability. To address this problem, ACCC avoids the

crossover between output impedance and input impedance by equivalently increasing the output capacitance size of the source converter, and does not introduce electrolytic capacitors, which does not affect the system lifetime.

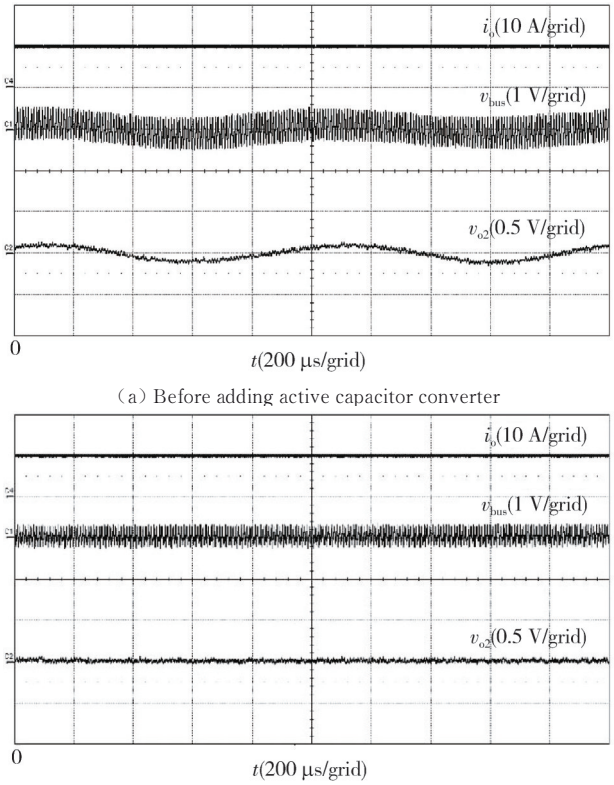

(a) Before adding active capacitor converter

(b) After adding active capacitor converter

Fig. 19 Control effect of ACCC under half load

4.2 Virtual resistor active damping control

ACCC ensures the stable operation of the cascade system by avoiding the amplitude crossover of Z_{o_S} and Z_{in_L} from the perspective of changing the output impedance of the source converter. Then, from the perspective of changing the input impedance of the load converter, a virtual impedance-based input impedance regulation strategy was proposed for the load converter to solve the instability problem of the cascade system[51-53].

As shown in Fig.20, it is a typical block diagram of a cascaded system, where $Z_{in\_L\_ori}(s)$ is the original input impedance of the load converter.

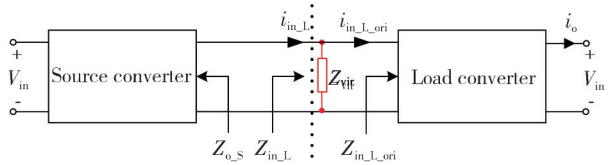

Fig. 20 Cascaded system after parallel virtual impedance

Within the voltage loop cut-off frequency f_{c_L}, the expression of $Z_{in\_L\_ori}(s)$ is

$$Z_{in\_L\_ori}(s)=-\frac{V_{bus}^2}{P_o}. \tag{26}$$

If a virtual impedance $Z_{vir}(s)$ is connected in parallel at the input end of the load converter, as shown in Fig.20, the equivalent input impedance $Z_{in\_L}(s)$ of the load converter is

$$Z_{in\_L}(s)=Z_{in\_L\_ori}(s)\|Z_{vir}(s)=\frac{Z_{in\_L\_ori}(s)Z_{vir}(s)}{Z_{in\_L\_ori}(s)+Z_{vir}(s)}. \tag{27}$$

Fig. 21 shows that there are two control methods for adjusting $Z_{in\_L}(s)$ to ensure the stability of the cascaded system from the perspective of input impedance.

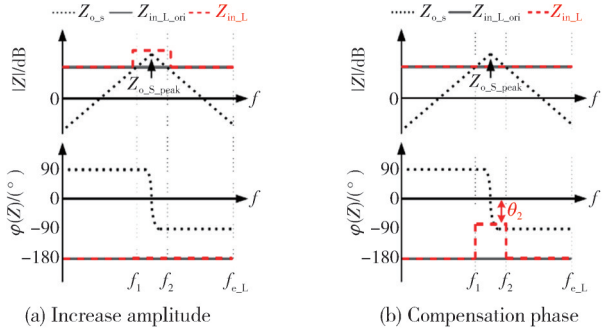

(a) Increase amplitude (b) Compensation phase

Fig. 21 Z_{in_L} adjustment methods

The first solution is to raise the amplitude of $Z_{in\_L}(s)$ between the crossover frequencies of $|Z_{o\_S}|$ and $|Z_{in\_L}|$, as shown in Fig.21(a).

The second is to compensate the phase of $Z_{in\_L}(s)$ between the crossover frequencies of $|Z_{o\_S}|$ and $|Z_{in\_L}|$ so that $|\phi(Z_{o\_S})-\phi(Z_{in\_L})|<180°$, as shown in Fig.21(b).

If the first method is adopted, Z_{in_L} can be designed to avoid the intersection of $|Z_{o\_S}|$ and $|Z_{in\_L}|$.

$$Z_{in\_L}(s)=\begin{cases}|Z_{in\_L1}|e^{j\theta_1}, & f\in[f_1,f_2],\\ Z_{in\_L\_ori}, & f\notin[f_1,f_2],\end{cases} \tag{28}$$

where f_1 and f_2 are the amplitude crossover frequencies of $Z_{o\_S}(s)$ and $Z_{in\_L\_ori}(s)$; $|Z_{in\_L1}|$ and θ_1 are $Z_{in\_L}(s)$ within the frequency range of $[f_1, f_2]$ after virtual impedance $Z_{vir}(s)$ is added, and thay are amplitude and phase, respectively.

Among them, $|Z_{in\_L1}|$ must satisfy

$$|Z_{in\_L1}|>|Z_{o\_S\_peak}|. \tag{29}$$

Combining Eqs. (28) — (29), the expression of $Z_{vir}(s)$ can be obtained by

$$Z_{vir}(s)=\begin{cases}\dfrac{-V_{bus}^2|Z_{in\_L1}|}{V_{bus}^2-|Z_{in\_L1}|P_o}, & f\in[f_1,f_2],\\ +\infty, & f\notin[f_1,f_2].\end{cases} \tag{30}$$

If the second method is adopted to compensate for the phase of $Z_{in\_L}(s)$, Z_{in_L} can be designed as

$$Z_{\text{in\_L}}(s)=\begin{cases}|Z_{\text{in\_L2}}|e^{j\theta_2}, & f\in[f_1,f_2],\\ Z_{\text{in\_L\_ori}}, & f\notin[f_1,f_2],\end{cases} \tag{31}$$

where $|Z_{\text{in\_L2}}|$ and θ_2 are the amplitude and phase of $Z_{\text{in\_L}}(s)$ after adjustment in the frequency range $[f_1, f_2]$, respectively, and θ_2 must satisfy

$$\theta\in(-90°,90°). \tag{32}$$

Combining Eqs. (31) — (32), the expression of $Z_{\text{vir}}(s)$ can be obtained by

$$Z_{\text{vir}}(s)=\begin{cases}\dfrac{V_{\text{bus}}^2|Z_{\text{in\_L1\_ori}}|e^{j\theta_2}}{V_{\text{bus}}^2+|Z_{\text{in\_L1\_ori}}|P_o e^{j\theta_2}}, & f\in[f_1,f_2]\\ +\infty, & f\notin[f_1,f_2].\end{cases} \tag{33}$$

To realize $Z_{\text{vir}}(s)$, a link with a transfer function of $1/Z_{\text{vir}}(s)$ can be introduced between the input voltage and input current of the load converter, as shown in Fig.22(a). Move the output of $1/Z_{\text{vir}}(s)$ in Fig.22(a) to the reference of the output voltage and adjust its transfer function to be

$$G_{\text{zin}}(s)=\frac{1}{Z_{\text{vir}}(s)}\cdot\frac{1+T_v(s)}{G_v(s)G_{\text{pwm}}(s)G_{\text{id\_OL}}(s)}, \tag{34}$$

where $T_v(s)=H_s(s)G_v(s)G_{\text{pwm}}(s)G_{\text{vd\_OL}}(s)$ is the loop gain of the load converter voltage closed loop.

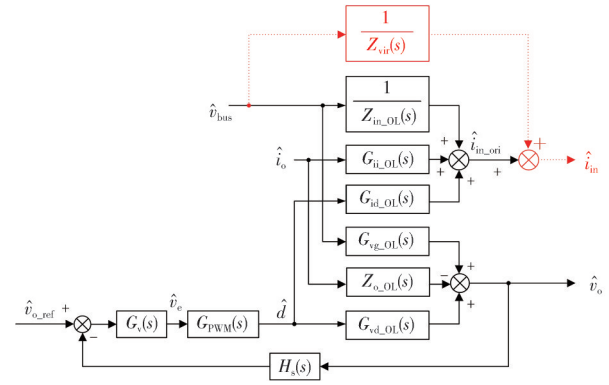

(a) Basic idea of input impedance adjustment strategy

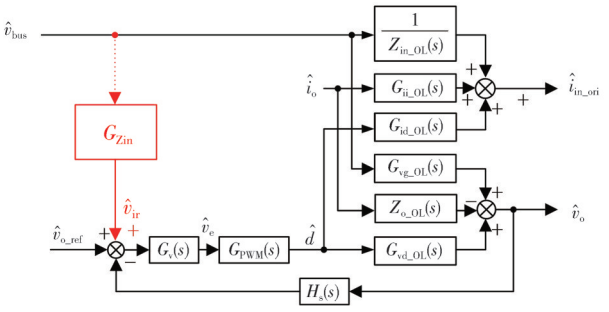

(b) Implementation of input impedance adjustment strategy

Fig. 22 Input impedance adjustment strategy

Fig. 22(b) shows the proposed input impedance adjustment strategy. Among them, $G_{\text{Zin}}(s)$ is an additional regulator introduced by the load converter to implement the input impedance adjustment strategy and is defined as an input impedance regulator below.

From Eqs. (30) — (34), to avoid the intersection of $|Z_{\text{o\_S}}|$ and $|Z_{\text{in\_L}}|$, $G_{\text{Zin}}(s)$ can be deduced by

$$G_{\text{zin}}(s)=-\frac{V_{\text{bus}}^2-|Z_{\text{in\_L1}}|P_o}{V_{\text{bus}}^2|Z_{\text{in\_L1}}|}\cdot\frac{1+T_v(s)}{G_v(s)G_{\text{pwm}}(s)G_{\text{id\_OL}}(s)}\cdot G_{\text{BPF}}(s), \tag{35}$$

where $G_{\text{BPF}}(s)$ is a band-pass filter, which consists of a second-order high-pass filter and a second-order low-pass filter in series, and it can be expressed as

$$G_{\text{BPF}}(s)=\frac{s^2}{s^2+\frac{\omega_1}{Q_H}s+\omega_1^2}\cdot\frac{\omega_2^2}{s^2+\frac{\omega_2}{Q_L}s+\omega_2^2}, \tag{36}$$

where $\omega_1=2\pi f_1$ is the characteristic corner frequency of the high-pass filter; $\omega_2=2\pi f_2$ is the typical corner frequency of the low-pass filter. Q_H and Q_L are the quality factors of the high-pass and low-pass filters, respectively.

To compensate for the phase of $Z_{\text{in\,L}}(s)$ between the crossover frequencies of $|Z_{\text{o\,S}}|$ and $|Z_{\text{in\,L}}|$, the expression of $G_{\text{Zin}}(s)$ can be inferred by Eqs. (33) and (34), that is

$$G_{\text{zin}}(s)=\frac{V_{\text{bus}}^2+|Z_{\text{in\_L\_ori}}|P_o e^{j\theta_2}}{V_{\text{bus}}^2|Z_{\text{in\_L\_ori}}|e^{j\theta_2}}\cdot\frac{1+T_v(s)}{G_v(s)G_{\text{pwm}}(s)G_{\text{id\_OL}}(s)}G_{\text{BPF}}(s). \tag{37}$$

In order to adjust the input impedance of the load converter, an input impedance adjustment strategy based on virtual resistance is proposed for the load converter. This strategy is equivalent to connecting a virtual resistor with the input end of the load converter, which can effectively adjust the amplitude and phase of the input impedance of the load converter and ensure that the DC microgrid with CPL is in a stable working state.

Also for the two-stage buck converter, when the system has stability problems that cause system voltage oscillation, the stability and dynamic characteristics of the system are observed after the virtual resistance active damping control is adopted.

The oltage waveform and dynamic characteristics are shown in the Fig.23. It can be seen from Fig.23(a) that the output voltage of the previous stage is in an oscillating state before active damping control is added. After the control is added, the output voltage of the latter stage is stable. Fig.23(b) compares the dynamic performance of cascade system with and without virtual resistance. The dynamic performance of the two systems is almost identical under the same input voltage jump. This example demonstrates how virtual resistor active damping control may increase system stability while

simultaneously providing good dynamic performance[17].

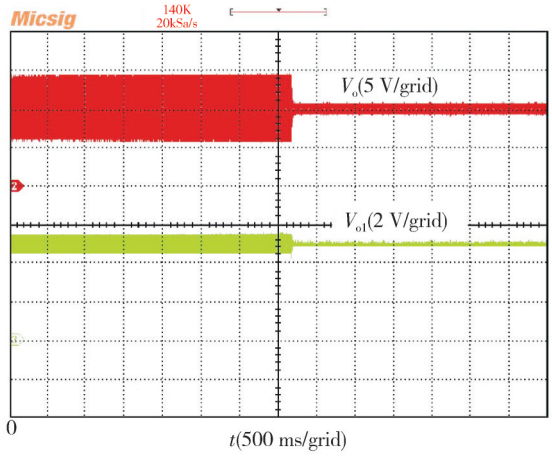

(a) Experimental waveforms before and after adding active damping control

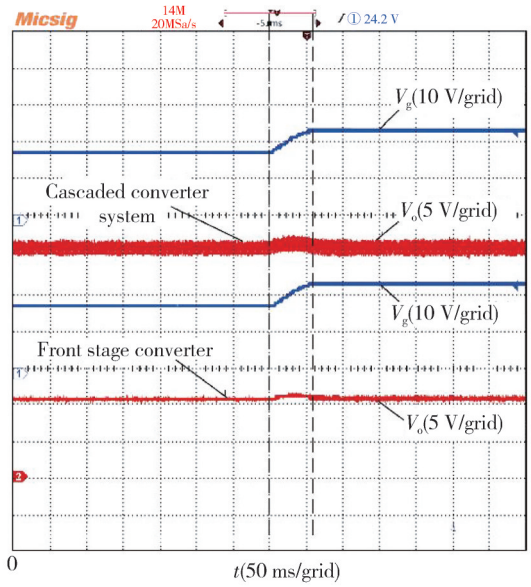

(b) Comparison of dynamic performance between cascaded system and stand-alone converter

Fig. 23 Voltage waveform and dynamic characteristics

Two widely used active control methods are proposed to adjust the output impedance of source converter and input impedance of load converter. Among them, ACCC not only solves the problem of stability, but also has good adaptive characteristics. The active damping control based on virtual resistance has good dynamic characteristics under this premise. These two methods can solve the CPL stability problem of unipolar microgrid well. However, there is no systematic stability analysis and control method for the stability of bipolar DC microgrids. The bipolar microgrid is one of the hot research directions in the future, and its stability problem has become an urgent problem to be solved.

5 Conclusions

Based on a comprehensive analysis of the existing DCDPS stability criteria, it can be seen that Middlebrook stability criterion and the stability criterion based on forbidden zone criterion are conservative, which will lead to some unnecessary costs at the beginning of the system design, including system performance decline, filter size increase, and bus capacitance increase. Although the T-SI and the general stability criteria can alleviate the inadequacies of the preceding criteria, they are both proposed based on the stability of the unipolar DC microgrid.

The stability of DC microgrid has always been the focus of research. There are mature stability analysis criteria and control methods for unipolar DC microgrid, but there is no complete theoretical system for bipolar DC microgrid. In terms of control methods to improve the stability of DC microgrids, the existing literatures mostly analyze the impedance characteristics of unipolar DC microgrid cascade systems and designs corresponding passive and active damping controls, while there is still a lack of complete stability analysis methods and control theories for the stability of bipolar DC microgrids with CPL.

Acknowledgement

This work was supported by National Natural Science Foundation of China (No. 51767015); Key Project of Natural Science Foundation of Gansu Province (No. 22JR5RA317); Tianyou Innovation Team Support Program of Lanzhou Jiaotong University (No. TY202009).

Declaration of conflicting interests

The authors have no conflict of interests related to this publication.

References

[1] LI X L, GUO L, WANG C S, et al. Key technologies of dc microgrids: an overview. Proceedings of the CSEE, 2016, 36(1): 2-17.

[2] LI X L, GUO L, GUO Z, et al. Coordinated control of multiple voltage balancers in a bipolar DC microgrid//2017 IEEE Power & Energy Society General Meeting, July 16-20, 2017, Chicago, IL, USA. New York: IEEE, 2017: 1-5.

[3] YANG M H, ZHANG R X, ZHOU N, et al. Unbalanced voltage control of bipolar DC microgrid based on distributed cooperative control//2020 15th IEEE Conference on Industrial Electronics and Applications (ICIEA), November 9-13, 2020, Kristiansand, Norway. New York: IEEE, 2020: 339-344.

[4] CAI W, YI F, COSOROABA E, et al. Stability optimization method based on virtual resistor and nonunity voltage feedback loop for cascaded DC-DC converters. IEEE Transactions on Industry Applications, 2015, 51(6): 4575-4583.

[5] HUANG X C, HE Z X, WU W H, et al. Stability analysis of converters cascade system in the hybrid AC/DC microgird and coordinative control. Proceedings of the CSEE, 2019, 39(5): 1432-1443.

[6] ZHANG Q J, ZHENG X L, LIU Y C, et al. Active damping suppression strategy for bus voltage oscillation in ship microgrid source-load cascade system. Proceedings of the CSU-EPSA, 2022, 34(3): 1-10.

[7] LIU X B, LIU N, SONG X T, et al. Large-signal stability criteria of AC/DC hybrid microgrid based on AC constant power loads. High Voltage Engineering, 2021, 47(10): 3441-3451.

[8] LIU Z K, WEI P, KONG L. Large-disturbance stability analysis of DC microgrid with constant power load and its transient voltage stability control strategy//2018 China International Conference on Electricity Distribution (CICED), September 17-19, 2018, Tianjin, China. New York: IEEE, 2018: 1686-1690.

[9] LUO W. Compound nonlinear control of DC/DC converter with constant power load. Guangxi: Guangxi University, 2021.

[10] ZHANG X, RUAN X B, ZHONG Q C. Improving the stability of cascaded DC/DC converter systems via shaping the input impedance of the load converter with a parallel or series virtual impedance. IEEE Transactions on Industrial Electronics, 2015, 62(12): 7499-7512.

[11] MENG J H, ZOU P G, WANG Y, et al. Small-signal modeling and parameter analysis of the DC microgrid based on flexible virtual inertia control. Transactions of China Electrotechnical Society, 2019, 34(12): 2615-2626.

[12] RAHIMI A M, EMADI A. Active damping in DC/DC power electronic converters: a novel method to overcome the problems of constant power loads. IEEE Transactions on Industrial Electronics, 2009, 56(5): 1428-1439.

[13] ZHANG X, ZHONG Q C, MING W L. Stabilization of cascaded DC/DC converters via adaptive series-virtual-impedance control of the load converter. IEEE Transactions on Power Electronics, 2016, 31(9): 6057-6063.

[14] PANG S Z, HUANGFU Y G, GUO L, et al. A novel wide stability control strategy of constant power load power converter based on the analysis of Lyapunov indirect method. Transactions of China Electrotechnical Society, 2017, 32(14): 146-154.

[15] WU M F, LU D D C. A novel stabilization method of LC input filter with constant power loads without load performance compromise in DC microgrids. IEEE Transactions on Industrial Electronics, 2015, 62(7): 4552-4562.

[16] HARNEFORS L, WANG X F, YEPES A G, et al. Passivity-based stability assessment of grid-connected VSCs-an overview. IEEE Journal of Emerging and Selected Topics in Power Electronics, 2016, 4(1): 116-125.

[17] HUANG Y, LIU H, MIAO Y, et al. Cascaded DC-DC converter stability control method based on paralleling virtual resistor. Transactions of China Electrotechnical Society, 2020, 35(18): 3927-3937.

[18] MIDDLEBROOK R. Input filter considerations in design and application of switching regulators//IEEE Power Electronics Specialists Conference, June 08-10, 1976, Cleveland, OH, USA. New York: IEEE, 1976.

[19] WILDRICK C M, LEE F C, CHO B H, et al. A method of defining the load impedance specification for a stable distributed power system. IEEE Transactions on Power Electronics, 1995, 10(3): 280-285.

[20] FENG X G, YE Z H, XING K, et al. Individual load impedance specification for a stable DC distributed power system//Fourteenth Annual Applied Power Electronics Conference and Exposition, March 14-18, 1999, Dallas, TX, USA. New York: IEEE, 1999: 923-929.

[21] RICCOBONO A, SANTI E. Comprehensive review of stability criteria for DC power distribution systems. IEEE Transactions on Industry Applications, 2014, 50(5): 3525-3535.

[22] SUDHOFF S D, GLOVER S F. Three-dimensional stability analysis of DC power electronics based systems//2000 IEEE 31st Annual Power Electronics Specialists Conference, June 23, 2000, Galway, Ireland. New York: IEEE, 2000: 101-106.

[23] SUDHOFF S D, CRIDER J M. Advancements in generalized immittance based stability analysis of DC power electronics based distribution systems//2011 IEEE Electric Ship Technologies Symposium, April 10-13, 2011, Alexandria, VA, USA. New York: IEEE, 2011: 207-212.

[24] SUDHOFF S D, GLOVER S F, LAMM P T, et al. Admittance space stability analysis of power electronic systems. IEEE Transactions on Aerospace and Electronic Systems, 2000, 36(3): 965-973.

[25] VESTI S, SUNTIO T, OLIVER J A, et al. Impedance-based stability and transient-performance assessment applying maximum peak criteria. IEEE Transactions on Power Electronics, 2013, 28(5): 2099-2104.

[26] WEI Y Q, LUO Q M, CHEN S, et al. DC current bus distributed power system and its stability analysis. IET Power Electronics, 2019, 12(3): 458-464.

[27] REN Y N, WANG X H, CHEN L, et al. A strictly sufficient stability criterion for grid-connected converters based on impedance models and gershgorin's theorem. IEEE Transactions on Power Delivery, 2020, 35(3): 1606-1609.

[28] ZHANG Y. Impedance modeling and stability analysis of medium voltage and low voltage DC distribution system. Jilin: Northeast Electric Power University, 2021.

[29] DU M. Research on stability of small signals in optical storage AC and DC microgrid based on impedance model .

Xi′an: Xi′an University of Technology, 2021.

[30] XIE W. Stability analysis and control strategies of DC microgrids. Beijing: North China Electric Power University, 2021.

[31] YANG X, ZHANG H, MA X. Stability margin monitoring for distributed power systems based on ESAC criterion. Transactions of China Electrotechnical Society, 2014, 24(8): 14-21.

[32] ZHANG Z R, XU Y W, YU L, et al. Parallel HVDC electric power system for more-electric-aircraft: State of the art and key technologies. Acta Aeronautica et Astronautica Sinica, 2021, 42(6): 12-25.

[33] ZHENG K, ZHOU L, ZHANG Q, et al. Stability analysis and parameter optimization design of photovoltaic grid-connected inverter under digital control. Transactions of China Electrotechnical Society, 2018, 33(8): 1802-1813.

[34] ZHANG X, RUAN X B, TSE C K. Impedance-based local stability criterion for DC distributed power systems. IEEE Transactions on Circuits and Systems I: Regular Papers, 2015, 62(3): 916-925.

[35] ZHANG X. On stability of DC distributed power system. Nanjing: Nanjing University of Aeronautics and Astronautics, 2014.

[36] RUAN X B. DC converter cascade systems: stability criteria and solutions. Nanjing: Nanjing University of Aeronautics and Astronautics, 2016.

[37] YOU X Y, LIU H P, MIAO Y R, et al. Stability analysis and active damping method of the bipolar DC system with constant power loads. Transactions of China Electrotechnical Society, 2022, 37(4): 918-930.

[38] CESPEDES M, XING L, SUN J. Constant-power load system stabilization by passive damping. IEEE Transactions on Power Electronics, 2011, 26(7): 1832-1836.

[39] ERICKSON R W, MAKSIMOVIĆ D. Fundamentals of power electronics. Cham: Springer International Publishing, 2020.

[40] REN X. Research on high efficiency high power density telecom power supply modules. Nanjing: Nanjing University of Aeronautics and Astronautics, 2008.

[41] WANG J. Research on interaction issues of nonlinear subsystems in distributed power system. Nanjing: Nanjing University of Aeronautics and Astronautics, 2010.

[42] YAO Y, ZHANG D, XU D. Output impedance optimization and stability for cascade DC/DC converter. Transactions of China Electrotechnical Society, 2009, 24(3): 147-152.

[43] CHEN P W, JIANG W W, RUAN X B, et al. Impedance explanation and resonance point sensitivity-based parameter design method of active damping applied to DC distribution system. Proceedings of the CSEE, 2021, 41(19): 6616-6630.

[44] LIU T F, TIAN Y J, JIANG Y X, et al. Active damped current observer oriented current sensorless feedback control for grid connected inverter. Proceedings of the CSEE, 2022, 42(19): 7182-7194.

[45] YANG L, ZHAO L H, CHEN X Q, et al. Robust active damping control for LCL-type shunt active power filters. IEEE Access, 2022, 10: 39456-39470.

[46] ZHAO W, CHEN P, CHEN X, et al. AC current feedback damping control strategy for VSC converter station in multi-terminal DC distribution system. Proceedings of the CSEE, 2021, 41(10): 3505-3517.

[47] ZHU X, MENG X. Stability analysis and research of active damping control method for DC microgrids. High Voltage Engineering, 2020, 46(5): 1670-1681.

[48] ZHANG X, RUAN X B, KIM H, et al. Adaptive active capacitor converter for improving stability of cascaded DC power supply system. IEEE Transactions on Power Electronics, 2013, 28(4): 1807-1816.

[49] WU T, RUAN X B. Characterization of input/output impedance specifications for dc distributed power system// International Telecommunications Energy Conference, New York: IEEE. 2006: 982-987.

[50] ZHANG X, RUAN X B, KIM H, et al. Adaptive active capacitor converter for improving stability of cascaded DC power supply system. IEEE Transactions on Power Electronics, 2013, 28(4): 1807-1816.

[51] ALI AZGHANDI M, BARAKATI S M, YAZDANI A. Impedance-based stability analysis and design of a fractional-order active damper for grid-connected current-source inverters. IEEE Transactions on Sustainable Energy, 2021, 12(1): 599-611.

[52] ZHANG Q J, LIU Q, LIU Y C, et al. Active damping control for energy storage system of DC microgrid. Chinese Journal of Power Sources, 2020, 44(10): 1538-1540.

[53] ZHOU L. Research on control method of active damper in weak grid with multiple grid-connected inverters. Harbin: Harbin Institute of Technology, 2021.

带恒功率负载的直流微电网稳定性控制研究综述

李 欣[1*], 邹俊南[2], 刘金辉[2]

1. 兰州交通大学 新能源与动力工程学院, 甘肃 兰州 730070;
2. 兰州交通大学 自动化与电气工程学院, 甘肃 兰州 730070

摘 要: 作为未来智能配用电系统的重要组成部分, 直流微电网具有能量转换效率高、能量传输密度大、不存在无功功率流动和并网同步等优势。然而, 恒功率负载(Constant power load, CPL)因其负阻特性, 会对直流微电网的稳定性产生不利影响, 造成系统电压振荡。因此, 带恒功率负载的直流微电网稳定性问题成为研究热点, 已有的直流微电网稳定性研究主要针对单极性直流微电网, 而针对双极性直流微电网的研究缺少系统论述。本文以单极性与双极性直流微电网为研究对象, 首先, 分析带恒功率负载的直流微电网稳定性。然后, 对目前直流微电网的稳定性判据进行归纳, 分析其研究趋势。在此基础上, 针对恒功率负载引起的稳定性问题, 从源变换器输出阻抗和负载变换器输入阻抗两个角度出发,对现有的控制方法归纳总结, 并将现有的控制方法总结归纳为有源控制方法和无源控制方法。最后, 对带恒功率负载的双极性直流微电网稳定性问题研究方向进行了展望。

关键词: 恒功率负载; 直流微电网; 电压平衡器; 稳定性判据; 级联系统; 虚拟电阻

引用格式: LI Xin, ZOU Junnan, LIU Jinhui. DC microgrid stability control with constant power load: a review. Journal of Measurement Science and Instrumentation, 2024, 15(4): 532-546.